Design of High-Lift Airfoils for Low Aspect Ratio Wings with Endplates

Ashok Gopalarathnam* and Michael S. Selig†
Department of Aeronautical and Astronautical Engineering
University of Illinois at Urbana-Champaign
Urbana, Illinois 61801

and
Frank Hsu‡
Advanced Engineering Center
Ford Motor Company
Dearborn, Michigan 48121

Abstract

High-lift multi-element airfoils for low-aspect ratio wings with endplates find application in race car rear wings used to generate high aerodynamic down force. Airfoils for such applications must not only generate maximum lift (to maximize the down force) but also must satisfy several geometric constraints imposed by the race rules. Induced effects arising as a result of the low aspect ratio determine the operating angle of attack at which the lift is to be maximized. This paper presents some of the challenges involved in designing such airfoils and briefly describes the design methodology adopted in the current work. A parametric study using a baseline two-element airfoil is then presented to illustrate some of the unusual results obtained as a consequence of satisfying the geometric constraints while maximizing the wing down force.

Nomenclature

c = chord
c_f = flap-element chord
c_m = main-element chord
c_t = total chord, $c_m + c_f$
C_l = airfoil lift coefficient, $l/\frac{1}{2}\rho V^2 w$
C_L = wing lift coefficient, $L/\frac{1}{2}\rho V_\infty^2 w$
g = ratio of the gap to the total chord
h = height of the constraint box
l = local "2D" lift per unit span
L = wing lift per unit span
$\vec{V}$ = local velocity vector at an airfoil section
$\vec{V}_\infty$ = freestream velocity vector
$\vec{w}$ = induced downwash velocity
w = width of the constraint box
α = angle of attack (angle between $\vec{V}$ and the x-axis)
α_i = induced angle of attack ($\alpha_i = -\alpha$)
δ_f = flap deflection
γ = angle of the airfoil in the box
ρ = density of air

Introduction

Most airfoils for practical aircraft applications are typically designed to achieve not only a desired aerodynamic performance but also satisfy certain geometric constraints. Examples are constraints on maximum thickness (for structural considerations), enclosed area (for fuel volume considerations) and trailing-edge geometry (for manufacturing considerations).

This paper describes a design methodology used in the design of two-element airfoils subject to some rather unusual constraints on the geometry. The objective was to design high-lift airfoils for race car rear wings to maximize the down force. As is well known,[1] increasing the aerodynamic down force increases the maximum lateral acceleration capability of the race car, allowing increases in cornering speeds. Geometric constraints on the airfoil imposed by the race rules, however, make this design problem challenging.

The current approach has been to use a multipoint inverse design code[2] for rapid and interactive design of two-element airfoils with desired inviscid velocity distributions and then analyze candidate designs using more computationally intensive viscous codes, in particular, MSES,[3] FUN2D[4] and NSU2D.[5] The results from the viscous codes were then used to provide feedback to the designer to further refine the performance of the airfoils. A MATLAB-based graphical user interface (GUI) was developed for interactively executing the various elements of the design code and for plotting the resulting airfoil along with the constraints on the geometry

*Graduate Research Assistant, 306 Talbot Laboratory. Student Member AIAA.

†Assistant Professor, 306 Talbot Laboratory. Senior Member AIAA.

‡Technical Specialist, MD 71, AEC 4507, 20000 Rotunda Drive.

AIAA Paper 97-2232
Presented at the AIAA 15th Applied Aerodynamics Conference
June 23–25, 1997, Atlanta, GA

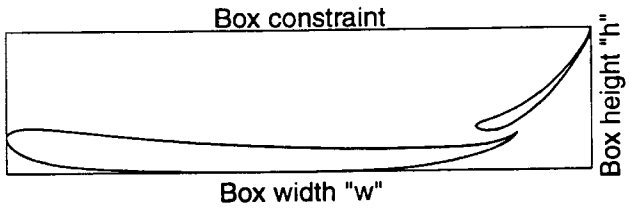

Fig. 1 Typical geometric constraints on indy car rear wings.

and the velocity distributions. The interface also allows graphical editing of the geometric parameters such as flap position, size, angle, etc. Such an interactive design tool was key to performing trade studies to assess the relative importance of the different design variables in maximizing the lift while satisfying the constraints.

This paper gives a brief description of typical geometric constraints imposed by the race rules, that is, the resulting restrictions that they impose on the design. The induced flow due the low aspect ratio wings is then discussed and followed by a brief description of the method used in the current work to determine the operating angle of attack of the airfoil. The next section compares the design philosophies commonly used in the design of high-lift multi-element airfoils and demonstrates why they may not be applicable when there are severe constraints on the geometry, such as those laid down by the race car rules. Finally, a three-part parametric study has been used to illustrate the design process, the challenges imposed on the design by the constraints and the rather unusual results obtained as a result of designing for high-lift while satisfying the geometric constraints. The parametric study presents results from both viscous and inviscid computations.

It should be noted that in this paper, except in Fig. 1, the airfoils will be shown "upside down," that is, flipped with respect to their orientation on the race car. Also, the airfoils will be referred to as having "high lift" rather than "high down force."

The Constraints on the Geometry

This section describes the constraints imposed on the rear wing geometry by the race rules. Typically, the rules specify that the geometry of the airfoil be constrained to a rectangular box referred to in this paper as the "constraint box" of specified dimensions.[6] Also specified are the maximum number of elements, the maximum span of the wing and the maximum dimensions of the endplates. The rules further restrict the bottom edge of the box to be parallel to the ground, making the freestream velocity vector $\vec{V}_\infty$ parallel to the bottom edge of the box (see Fig. 1). Figure 1 shows a two-element airfoil in a typical indy car rear wing box constraint.

Table 1: Dimensions of the wing and endplates as used in the current study.

Wing span = 43 in.
Box height h = 5 in.
Box width w = 20 in.
Box h/w = 0.25
Wing aspect ratio = 2.15
Endplate chord = 20 in.
Endplate height = 8 in.
Effective wing aspect ratio = 2.57

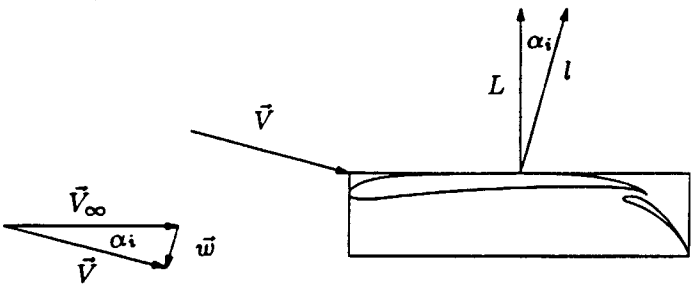

Fig. 2 Finite wing corrections.

It is to be noted, however, that the geometric constraints usually vary from year to year. For the present study, two-element airfoils have been considered, and a box size h/w ratio of 0.25 has been assumed, along with the wing and constraint box dimensions listed in Table 1. The endplate size has been assumed to be identical to that of the constraint box.

Since the maximum span as limited by the race rules results in a very low aspect ratio wing, the downwash induced by the trailing vortex system is quite high and increases with increasing wing lift. As demonstrated in Fig. 2, the low aspect ratio of the wing, coupled with the restriction that the bottom edge of the box must be parallel to the ground, results in a highly negative operating angle of attack for the airfoil. Consequently, the design problem becomes one of maximizing the lift at a *negative* angle of attack.

While there is no direct contribution to the lift from the endplates, the endplates result in an effective increase in the aspect ratio, and hence a less negative operating angle of attack. Thus, they play an "indirect" role in increasing the maximum lift. In the current work, the effect of endplates has been accounted for by increasing the geometric aspect ratio of the wing based a simple 3-D model of a short aspect wing with endplates modeled according to Ref. 7. Table 1 lists the effective aspect ratio used in the present study.

Determination of Operating Condition

The induced downwash corresponding to any given value of wing lift can be computed using the finite-wing theory for high-lift, low aspect-ratio wings documented in Ref. 8. This theory assumes an elliptic lift distribution, but differs from the conventional lifting-line theory for elliptically loaded wings in that the trailing vortex wake is assumed to trail not in the direction of the freestream velocity vector $\vec{V}_\infty$, but in the direction of the local velocity vector $\vec{V}$. The wake is therefore deflected down from the horizontal by an angle equal to the induced downwash angle α_i.

Figure 2 illustrates the effect of the induced downwash on the operating angle of attack of the airfoil. Consider the two-element airfoil in the constraint box in Fig. 2. Since the wing is generating positive lift, there is an induced downwash $\vec{w}$ that results in the local velocity vector $\vec{V}$ as shown in the figure. As can be seen from the figure, the assumption that the trailing vortex wake is at an angle α_i to the freestream, results in the downwash velocity vector $\vec{w}$ being tilted at an angle α_i to the vertical. As a consequence, the local velocity vector $\vec{V}$ has a smaller magnitude than that of the freestream velocity vector $\vec{V}_\infty$. Also seen in Fig. 2 is that the angle of attack α relative to the x-axis is exactly equal to the induced angle α_i, but with the sign reversed.

Figure 3 shows the variation of airfoil C_l and wing C_L corresponding to various values of the induced downwash angle α_i, as a result of satisfying the finite-wing theory. The airfoil C_l is less than the wing C_L not only because the wing lift per unit span L is smaller than the local lift per unit span l, but also because the local velocity vector $\vec{V}$ is smaller in magnitude than the freestream velocity $\vec{V}_\infty$. Figure 4 shows the variation of the wing lift coefficient C_L with the airfoil lift coefficient C_l, obtained as a result of satisfying the finite-wing theory.

To illustrate the determination of the operating angle of attack for any airfoil in the constraint box, consider the two-element airfoil of Fig. 2. This airfoil can be analyzed to obtain the C_l vs. α variation, where α is defined relative to the x-axis (the top edge of the box, in this case). The C_l vs. α curves for this airfoil as obtained from 1) an inviscid analysis using MCARF, a panel method, and 2) a viscous analysis using FUN2D, a Navier-Stokes code, are plotted in Fig. 5, along with the airfoil C_l vs. α_i obtained as a result of satisfying the finite-wing theory. The operating angles of attack, as shown in the figure, are the intersections of the curves from analysis and finite-wing theory. As seen in Fig. 5, the operating condition for inviscid flow is different from that for viscous flow.

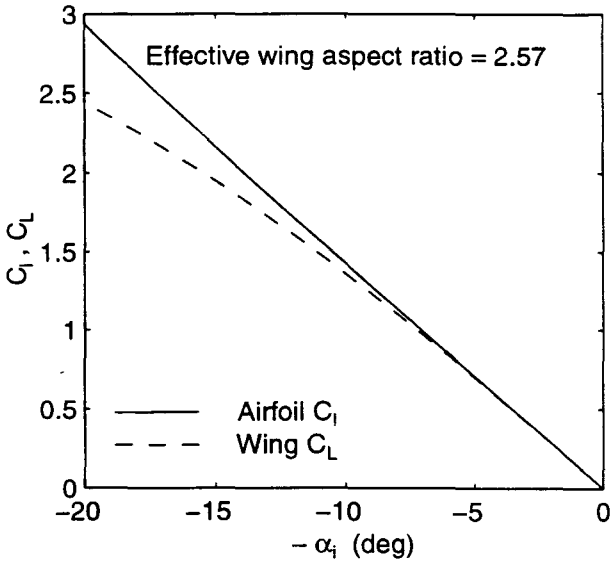

Fig. 3 Variation of airfoil C_l and wing C_L with induced downwash angle.

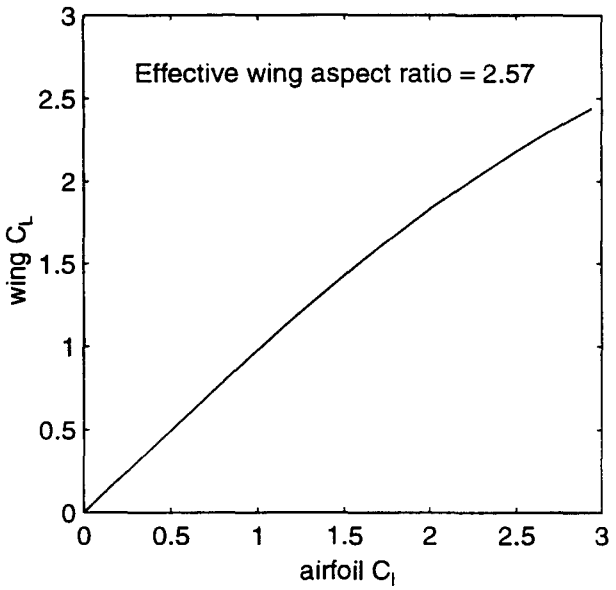

Fig. 4 Variation of wing C_L with airfoil C_l.

Design Methodology

The design methodology in the current work has been to use a multipoint inverse design code for multi-element airfoils[2] coupled with a custom MATLAB-based graphical user interface (GUI) for rapid and interactive design of two-element airfoils with desired inviscid velocity distributions. Candidate designs are then analyzed using more computationally intensive viscous codes, in particular, MSES,[3] FUN2D[4] and NSU2D.[5] The results from the viscous codes were then used to provide feedback to further refine the performance of the airfoils.

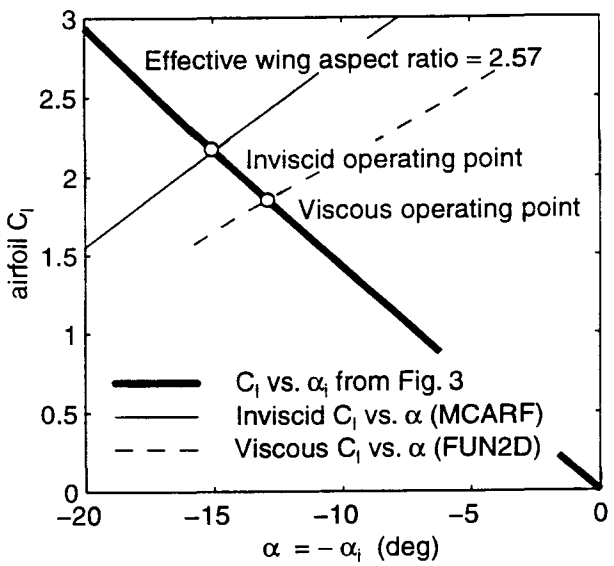

Fig. 5 Illustration of the method used to determine the operating angle of attack.

The inverse design method of Ref. 2 for multi-element airfoils uses a hybrid approach by coupling an isolated-airfoil multipoint design code (PROFOIL[9]) to generate each element of the multi-element airfoil and a two-dimensional panel method (MCARF[10]) to analyze the multi-element airfoil. The method makes use of the observation that changes in the velocity distribution over the elements in isolation result in remarkably similar changes in the velocity distributions over the corresponding elements of the multi-element airfoil. Newton iteration is used to adjust the velocity distributions over the airfoils in isolation to obtain desired multi-element velocity distributions. Figure 6 shows an overview of the inverse design method, more details of which are documented in Ref. 2.

A custom MATLAB-based GUI was developed to enable the designer to interactively execute the various elements of the design code and subsequently plot the resulting airfoil geometries and the corresponding velocity distributions along with the geometric constraints. While the multi-element inverse method has both PROFOIL and MCARF embedded in it, the GUI provided the designer with additional capability of executing either PROFOIL to generate/modify any of the two elements of the airfoil, or MCARF to obtain a panel-method solution for the two-element airfoil. In addition, the GUI has several features that allow the designer to edit the geometry of the multi-element airfoil using the cursor, enabling several parametric studies to be performed in a rapid and interactive manner. All of the two-element airfoils used in the parametric studies that follow were generated using this GUI.

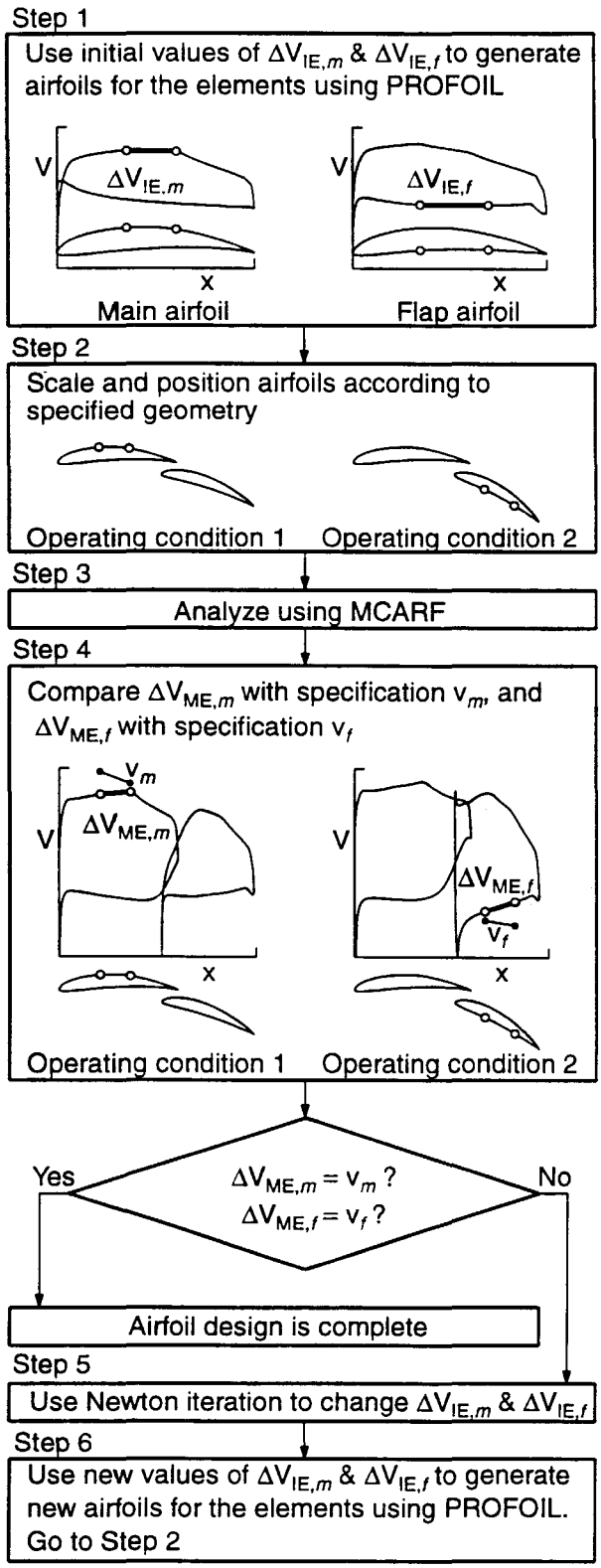

Fig. 6 An overview of the inverse design method for multi-element airfoils.

While the GUI allowed rapid design of several candidate two-element airfoils with desired inviscid velocity distributions subject to geometric constraints, more computationally intensive codes such as MSES,[3] FUN2D[4] and NSU2D[5] were used to obtain the viscous behavior of these airfoils. In this paper, only the results from FUN2D are presented.

High Lift Design Philosophy

This section describes briefly the design philosophies used in conventional high-lift airfoil design and demonstrates that such philosophies are not effective when the airfoil is required to maximize the lift, while satisfying the box constraint. A new design philosophy is then proposed for the design of high-lift airfoils for the current application.

Conventional high-lift single and multi-element airfoils, which do not have any restriction on the operating angle of attack, are typically designed so that the velocity distributions on the upper surface of each element has the highest possible rooftop velocity over the forward portion, followed by a Stratford pressure recovery to keep the turbulent boundary layer close to separation, with high aft-loading at the trailing-edge.[11,12,13]

Airfoils designed using such a philosophy do not perform well on indy car rear wings that have to maximize the lift while operating at a highly negative angle of attack. To demonstrate this point, a two-element airfoil was designed to have a $C_{l,max}$ of approximately 4.5. Figure 7a shows this two-element airfoil and the inviscid velocity distribution at the high-lift condition corresponding to a C_l of 4.5. Figure 7b demonstrates that when this airfoil is constrained to operate within the box, the C_l drops to 1.59 owing to the negative operating angle of attack.

Therefore, a new high-lift design philosophy has been developed for the current application. The philosophy is to have as high a suction peak as possible at the leading edge of the main element upper surface, and as high an aft-loading as possible at the trailing edge while still satisfying the geometric constraints. The flap is used to load the trailing edge of the main element. Figure 8 shows a two-element airfoil designed with such a philosophy and the inviscid velocity distribution corresponding at the operating condition. The inviscid C_l for this airfoil is approximately 2.2 while satisfying the box constraints.

Parametric Study

In this section, a three-part parametric study is presented to illustrate some of the unusual results obtained as a consequence of satisfying the geometric constraints. The two-element airfoil shown with the constraint box

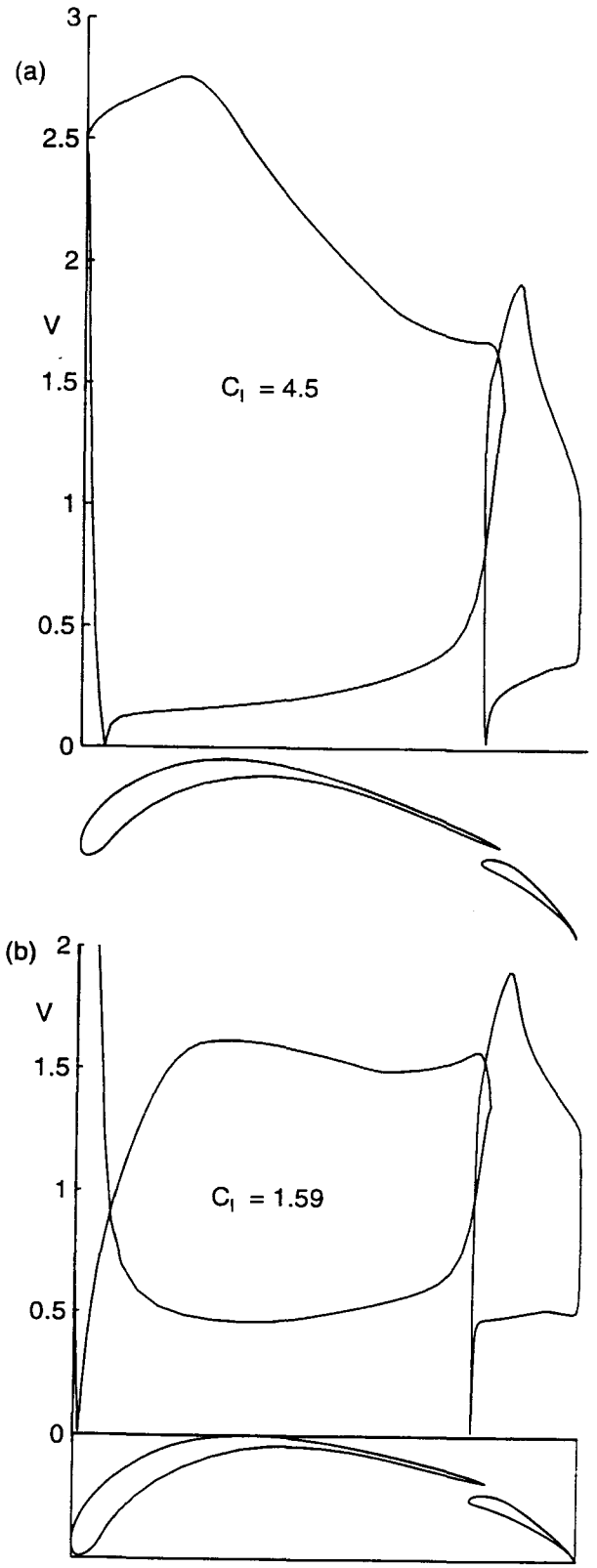

Fig. 7 Airfoil designed for high-lift (a) at high-lift condition without box constraint (b) operating with box constraint.

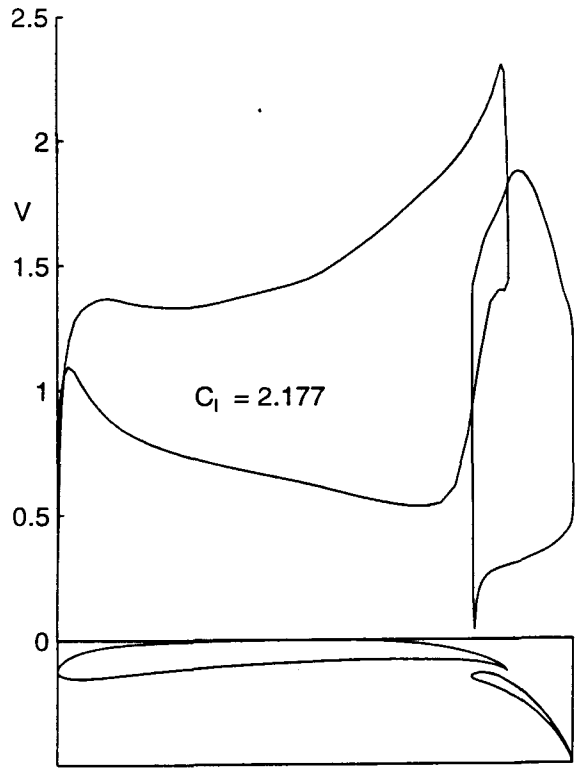

Fig. 8 Airfoil designed to produce high-lift while satisfying box constraint.

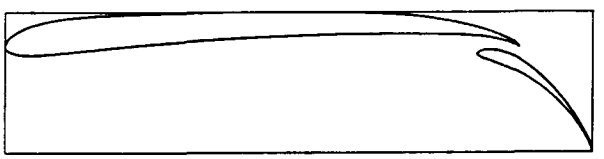

Fig. 9 Two-element airfoil used as the baseline for the parametric study.

in Fig. 9 is used as the baseline airfoil for the study. The first part of the parametric study focuses on the effect of the angle γ of the airfoil in the box, the second part on the effect of the flap-to-main chord ratio c_f/c_m and the third part on the gap g between the main and the flap elements as a ratio of the sum of the total chord c_t.

In all three parts, results from both inviscid and viscous analyses are presented. Inviscid computations were performed using the GUI to execute the panel method MCARF. The execution time was less than 5 seconds to analyze an airfoil over a range of angles of attack.

The viscous computations were performed using FUN2D, a two-dimensional unstructured Navier-Stokes code.[4] All the airfoils in the parametric study were analyzed at a Reynolds number (based on the box width w) of 2.4×10^6 and a Mach number of 0.2, which are the design conditions for the rear-wing airfoils. Figure 10

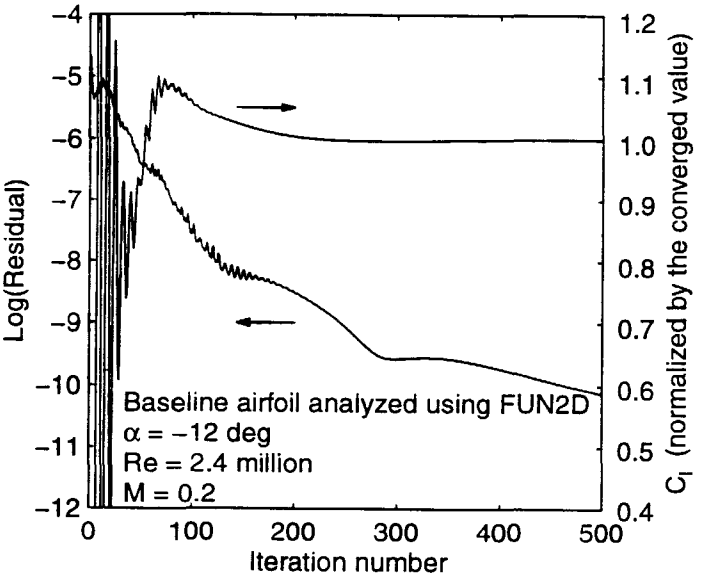

Fig. 10 Residual plot and convergence of the normalized C_l.

shows the convergence of the airfoil C_l and residual after 500 iterations (in this case, for the baseline airfoil at an angle of attack of -12 deg relative to the x-axis). For a typical case, a three-level multi-grid analysis was performed, with approximately 50,000 nodes for level 1, approximately 20,000 nodes for level 2, and approximately 10,000 nodes for level 3. Typical run times for 500 iterations were approximately 40 min on a Cray C90 for a solution at a single angle of attack.

Effect of the Angle of the Airfoil in the Box

In this part of the study, the gap (non-dimensionalized by the sum of the chord of the main and flap elements) and the flap-to-main chord ratio have been maintained constant. The angle γ of the airfoil in the box as defined by the angle between the chord line of the main element and the x-axis has been varied to study its effect on the wing C_L. In all cases, the two-element airfoils were scaled to the largest chord while satisfying the box constraint at the specified value of γ.

Figures 11a–c show the baseline airfoil having γ = 0.2 deg, two airfoils resulting from $\gamma = -4.8$ and 5.4 deg, and the corresponding velocity distributions. Figure 12 shows the variation of the wing C_L with γ from both viscous and inviscid computations at their respective operating conditions. As seen from the figure, while there is negligible change in the wing C_L with increasing values of γ above the baseline, there is a sharp decrease in the C_L for values of γ less than the baseline. The reason for this behavior can be deduced by examining the variation of the airfoil scale factor (factor by which the airfoil has been scaled down from the baseline case) and

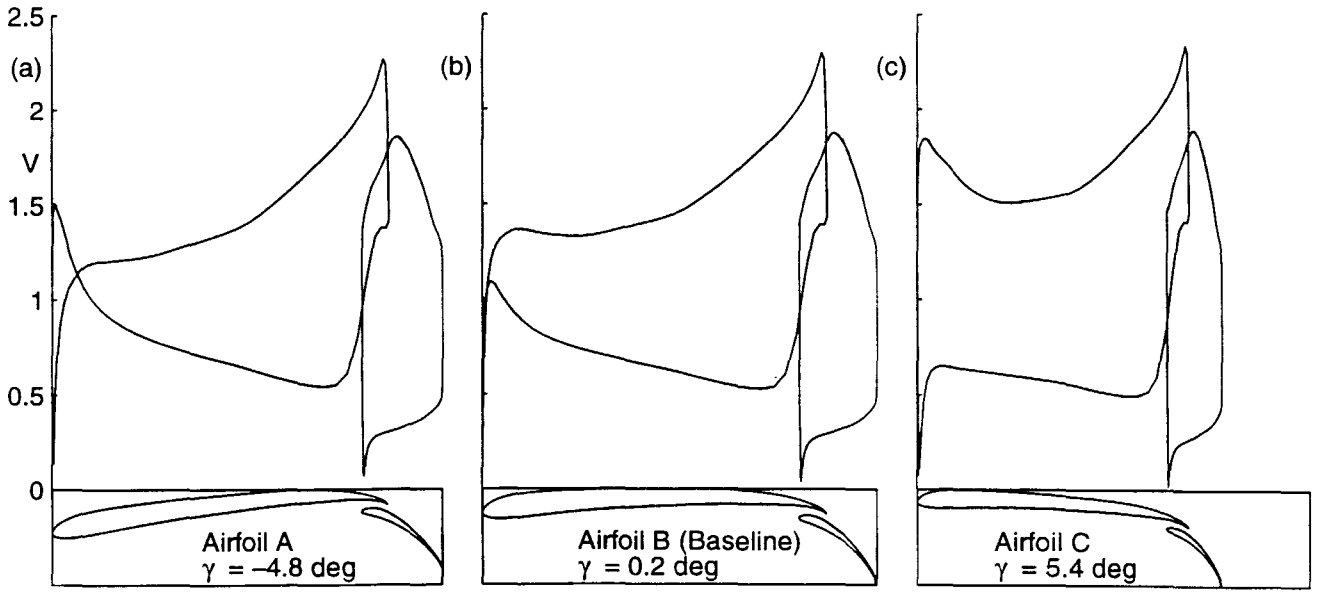

Fig. 11 The airfoils and inviscid velocity distributions resulting from (a) $\gamma = -4.8$ deg, (b) $\gamma = 0.2$ deg and (c) $\gamma = 5.4$ deg.

the operating angle of attack with γ. These variations are shown in Figs. 13a and b. For values of γ greater than that of the baseline, the scale factor of the airfoils decreases rapidly. This decrease, however, is nearly offset by increasing values of the operating angle of attack, resulting in a nearly constant lift for values of γ greater than that of the baseline. On the other hand, for values of γ less than that of the baseline, both the operating angle of attack and the scale factor decrease, resulting in the sharp decrease in the wing lift.

Another remarkable result of this parametric study is that the trends in variation in wing C_L with γ for both the inviscid and viscous computations are almost identical. The reason for the similarity in the trends is that the effect of γ is driven almost entirely by the shape of the constraint box. The similarity in the trends demonstrate the usefulness of selecting "promising" candidate airfoil sections using the rapid, interactive inviscid design method before performing highly intensive viscous analyses to select the "best" candidates.

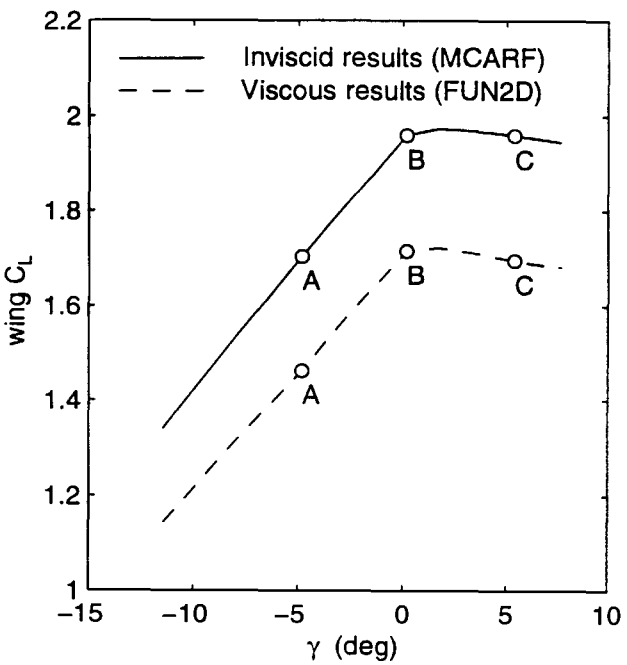

Fig. 12 Effect of γ on wing C_L.

Effect of the Flap-to-Main Chord Ratio

For the second part of the study, the angle γ of the airfoil in the box, the total chord ($c_t = c_m + c_f$) and gap (non-dimensionalized by c_t) have been maintained constant, and the flap-to-main chord ratio c_f/c_m has been varied. In each case, the trailing edge of the flap was fixed at the bottom-right corner of the box, and the flap angle δ_f relative to the main element chord was varied until the specified gap was obtained.

Figures 14a–c show the baseline airfoil having $c_f/c_m = 0.30$, two airfoils with c_f/c_m values of 0.25 and 0.35, and the corresponding velocity distributions. The variation in the wing C_L from both viscous and inviscid computations with c_f/c_m is shown in Fig. 15. Figure 16 shows the variation of δ_f with the flap-to-main chord ratio. It is seen that the inviscid computations show a

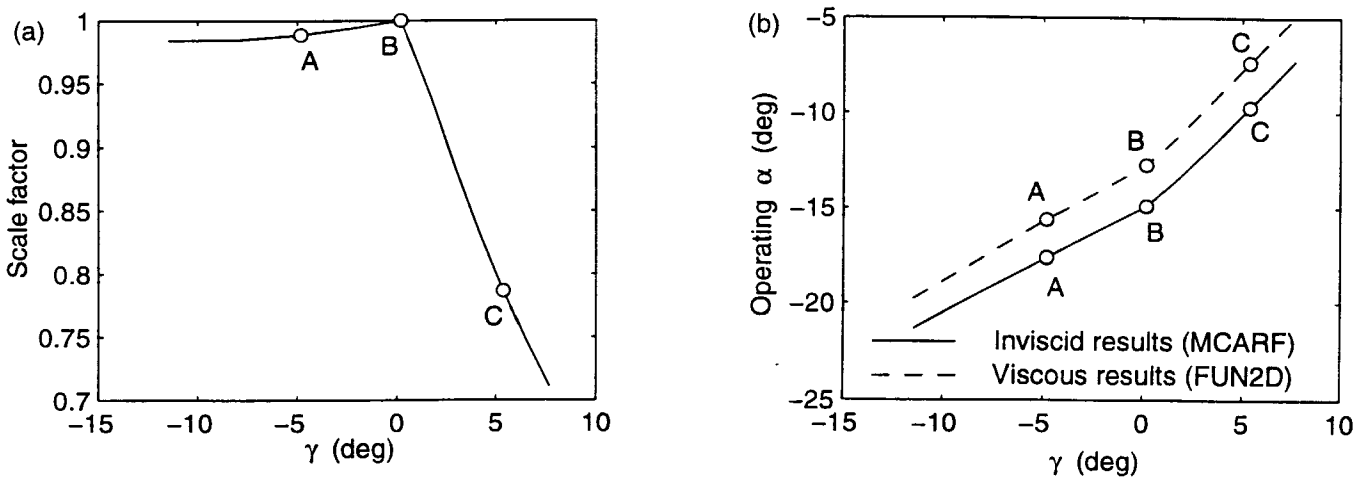

Fig. 13 Variation of (a) scale factor and (b) operating α with γ.

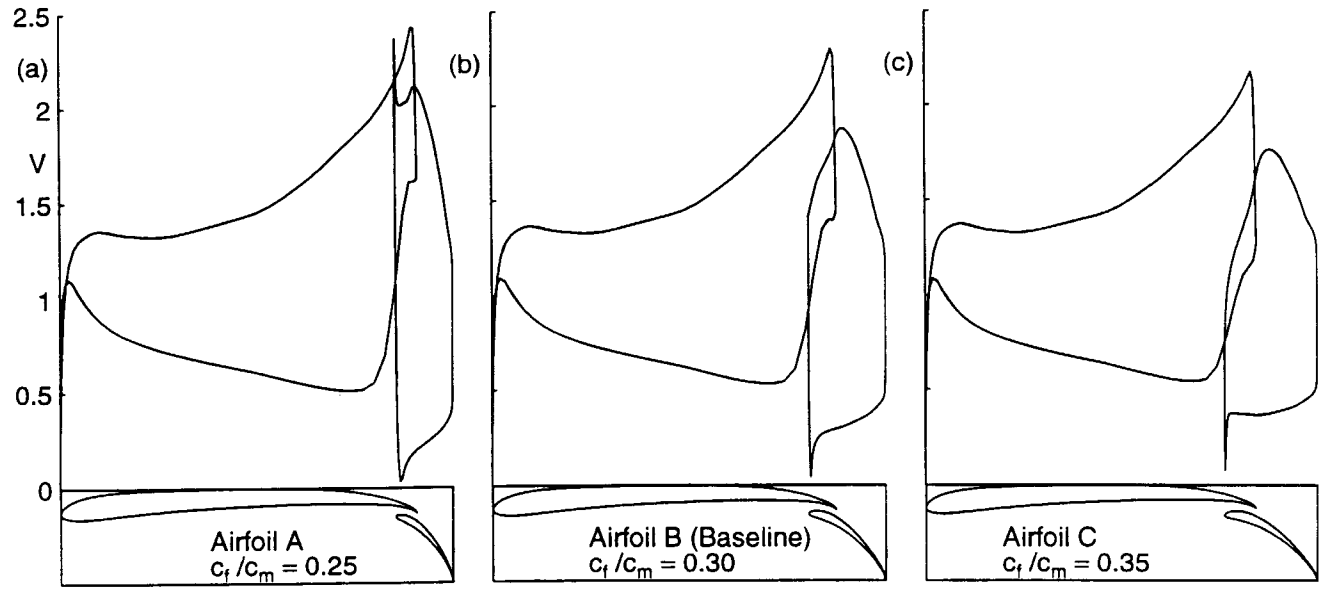

Fig. 14 The airfoils and inviscid velocity distributions resulting from (a) $c_f/c_m = 0.25$, (b) $c_f/c_m = 0.30$ and (c) $c_f/c_m = 0.35$.

monotonically increasing trend for the wing C_L with decreasing c_f/c_m. The reason for this behavior can be understood by observing that, in this study, the flap angle δ_f increases with decreasing values of c_f/c_m. The inviscid analyses are driving the design to a configuration where the two-element airfoil nearly "crawls" along the top and right-hand edges of the constraint box. For very high values of δ_f, however, the flow begins to separate, resulting in an optimum value of c_f/c_m below which the wing C_L decreases because of separation resulting from the high flap deflections.

This study demonstrates that while the inviscid design tool is good for rapidly generating candidate airfoils, there is clearly a need for viscous analysis codes to select design parameters that maximize the lift.

Effect of the Gap

For this part of the study, the angle γ of the airfoil in the box and flap-to-main chord ratio c_f/c_m have been maintained constant. The ratio gap-to-total-chord g has been altered. In each case, the trailing edge of the flap was fixed at the bottom-right corner of the constraint box, and the flap angle was varied until the specified

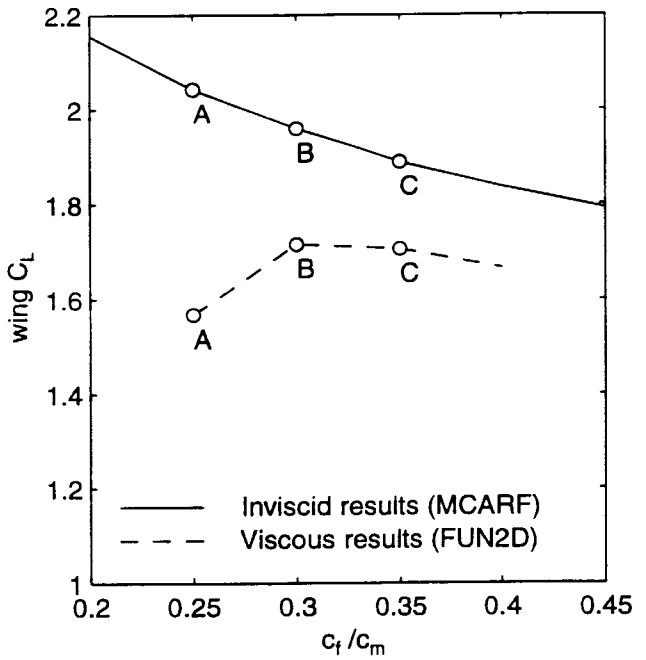

Fig. 15 Effect of c_f/c_m on wing C_L.

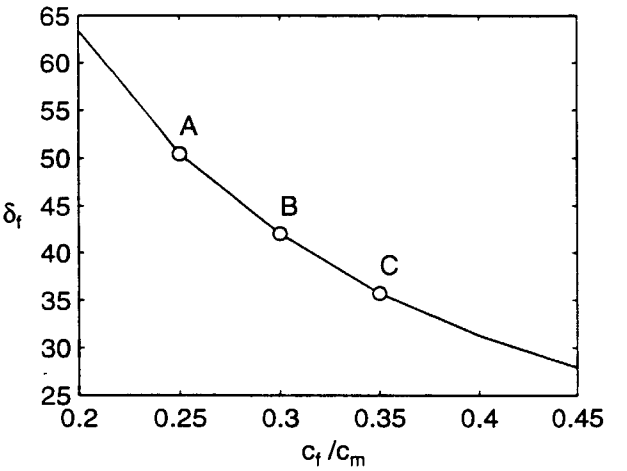

Fig. 16 Variation of δ_f with flap-to-main chord ratio.

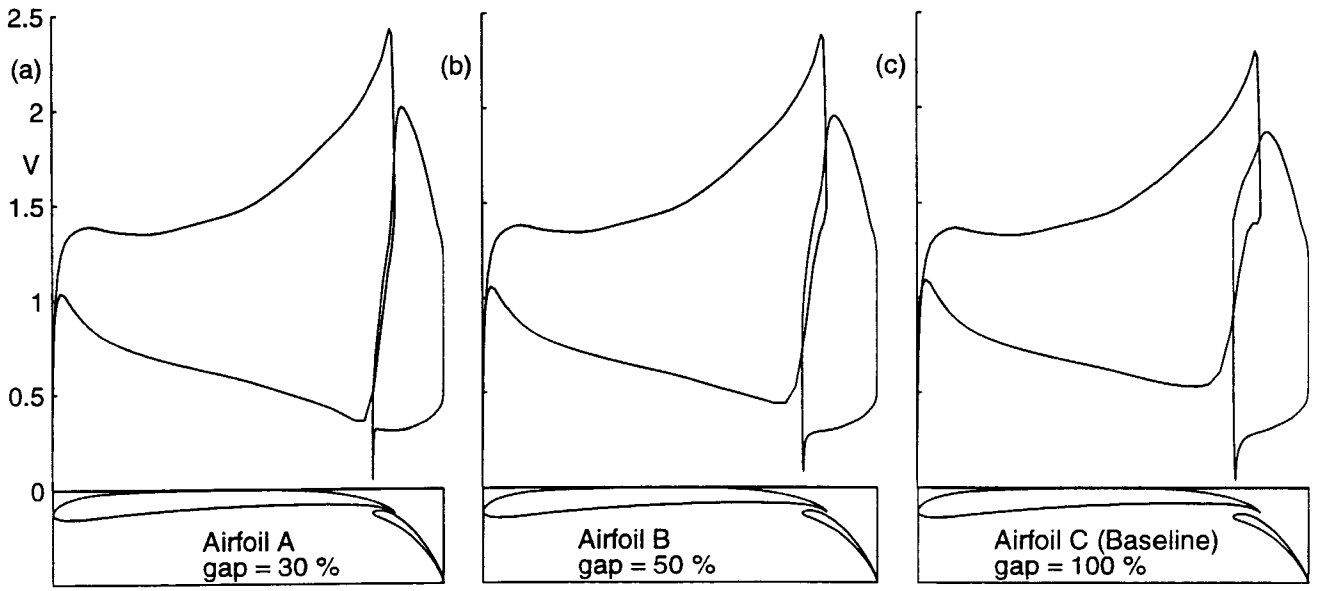

Fig. 17 The airfoils resulting from (a) gap = 30%, (b) gap = 50% and (c) gap = 100% of the gap of the baseline airfoil.

gap was obtained.

Figure 17a–c shows the baseline airfoil having $g = -0.02$, and two airfoils with gap values of 50% and 30% of the gap of the baseline airfoil. The variation in the wing C_L with gap from both inviscid and viscous computations is shown in Fig. 18. As can be expected, the inviscid wing C_L increases with decreasing gap values. When the gap becomes very small, however, viscous effects such as confluent boundary layers and wakes tend to reduce the lift generated, resulting in a value of gap below which there is a decrease in the wing C_L. This study again emphasizes the importance of performing

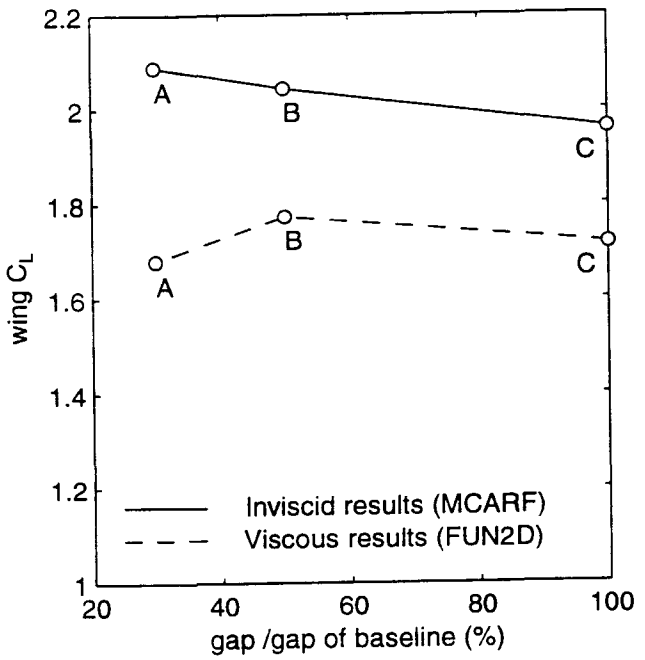

Fig. 18 Effect of gap on wing C_L.

viscous computations in designing two-element airfoils for high-lift.

Conclusions

The paper has dealt with issues involved in designing high lift airfoils for race car applications. The severe constraints on the geometry of the airfoil imposed by the race rules coupled with the low aspect ratio wing present some unusual design challenges for the airfoil. As demonstrated in the paper, the geometric constraints result in the airfoil having to produce high-lift while operating at a highly negative angle of attack. The conventional approach to designing for high lift without an angle of attack constraint, that is, not subject to a box constraint, has little bearing on the current approach.

A methodology has been developed for designing such airfoils. The method uses a graphical user interface to drive an inverse airfoil design method for designing multi-element airfoils to achieve a desired inviscid behavior. This interface allows for rapid, interactive design of several candidate airfoils that satisfy the geometric constraints. Computationally intensive viscous methods are then used to analyze the viscous performance of candidate airfoils.

A three-part parametric study has been presented, which examines the effect of the angle of the airfoil in the box, the flap-to-main chord ratio and the gap on the wing lift. Results from both inviscid and viscous computations are presented. The parametric study shows some of the unusual results obtained as a result of satisfying the geometric constraints. In addition, the study demonstrates the effectiveness of using rapid inviscid inverse design tools to select candidate airfoils, which can then be analyzed using more computationally intensive viscous codes to select the "best" airfoil.

Acknowledgments

The support of the Ford Motor Company is gratefully acknowledged. Also, Dimitri Mavriplis (Scientic Simulations) and Chun-Keet Song (University of Illinois) are thanked for their efforts in running the Navier-Stokes code NSU2D, the results of which were not presented in this paper yet nevertheless supported the conclusions of this work.

References

[1]Katz, J., *Race Car Aerodynamics,* Robert Bentley Publishers, Cambridge, MA, 1995.

[2]Gopalarathnam, A. and Selig, M.S., "A Multipoint Inverse Method for Multi-Element Airfoil Design," AIAA Paper 96-2396, June 1996

[3]Drela, M., "Design and Optimization Method for Multi-Element Airfoils," AIAA Paper 93-0969, Feb. 1993.

[4]Anderson, W.K., and Bonhaus, D.L., "Navier-Stokes Computations and Experimental Comparisons for Multielement Airfoil Configurations," AIAA Paper 93-0645, Jan. 1993

[5]Valarezo, W.O. and Mavriplis, D.J., "Navier-Stokes Applications to High-Lift Airfoil Analysis," AIAA Paper 93-3534, Aug. 1993.

[6]Anonymous, 1997 CART Rule Book, Championship Auto Racing Teams, Inc., Troy, MI, 1997.

[7]Schlichting, H. and Truckenbrodt, E., "Aerodynamics of the Airplane," McGraw-Hill International Book Company, New York, 1979.

[8]McCormick, B.W., Jr., "Aerodynamics of V/STOL Flight," Academic Press, New York, 1967.

[9]Selig, M.S. and Maughmer, M.D., "A Multi-Point Inverse Airfoil Design Method Based on Conformal Mapping," *AIAA Journal*, Vol. 30, No. 5, 1992, pp. 1162–1170.

[10]Morgan, H.L., Jr., "A Computer Program for the Analysis of Multi-Element Airfoils in Two-Dimensional, Subsonic, Viscous Flow," NASA SP-347, March 1975.

[11]Smith, A.M.O., "High-Lift Aerodynamics," *Journal of Aircraft*, Vol. 12, No. 9, 1975, pp. 501–530.

[12]Liebeck, R., "Subsonic Airfoil Design," in *Applied Computational Aerodynamics*, P.A. Henne (Ed.), Vol. 125, AIAA, Washington, DC, 1990, pp. 133–165.

[13]Selig, M.S. and Guglielmo, J.J., "High-Lift Low Reynolds Number Airfoil Design," *Journal of Aircraft*, Vol. 34, No. 1, 1997, pp. 72–79.